This is a preprint, the final version is subject to change, of the American Mineralogist (MSA)
Cite as Authors (Year) Title. American Mineralogist, in press.
DOI: https://doi.org/10.2138/am-2020-7270

Revision 1-clean version

The occurrence, origin and fate of water in chromitites in ophiolites

Ben-Xun Su[1, 2, 3*], Paul T. Robinson[1], Chen Chen[1, 2, 3], Yan Xiao[2, 4], Frank Melcher[5], Yang Bai[1, 2, 3], Xiao-Yan Gu[6], Ibrahim Uysal[7], Davide Lenaz[8]

[1] Key Laboratory of Mineral Resources, Institute of Geology and Geophysics, Chinese Academy of Sciences, Beijing 100029, China

[2] Innovation Academy for Earth Science, Chinese Academy of Sciences, Beijing 100029, China

[3] University of Chinese Academy of Sciences, Beijing 100049, China

[4] State Key Laboratory of Lithospheric Evolution, Institute of Geology and Geophysics, Chinese Academy of Sciences, Beijing 100029, China

[5] Chair of Geology and Economic Geology, Montanuniversität Leoben, Leoben 8700, Austria

[6] School of Earth Sciences, Zhejiang University, Hangzhou 310027, China

[7] Department of Geological Engineering, Karadeniz Technical University, 61080-Trabzon, Turkey

[8] Department of Mathematics and Geosciences, University of Trieste, Via Weiss 8, 34122 Trieste, Italy

Words: 3899

Figures: 8

Tables: 4

Supplementary Tables: 1

Abstract

* Corresponding author: BX Su, subenxun@mail.igcas.ac.cn.

This study presents petrological investigations and mineral chemistry of several Tethyan ophiolites to reveal occurrence, origin and fate of water in podiform chromitites. The results show that clinopyroxene and olivine in chromitites have H_2O contents of 801-366 ppm and 53-17 ppm, respectively. The highest water contents of olivine occur in massive chromitite and the lowest always in the clinopyroxene-bearing ores because much of the available hydrous fluid was taken up by the clinopyroxene during crystallization. The major and trace elemental and Li isotopic compositions of clinopyroxene associated with chromite and olivine in podiform chromitites indicate formation from a mixture of surface hydrous fluids on chromite grains and evolved melts from which olivine crystallized. The hydrous fluids initially originated from dehydration of subducting slab revealed by Li isotopic compositions of clinopyroxene and olivine in the chromitites. High fluid/rock ratios facilitated concentration of chromite to form chromitite, suppressing crystallization of olivine. The hydrous fluids that were collected on the chromite grain surface during crystallization allow chromite grains to rise via decreasing density in form of bubbles, thus promoting their gathering and concentration. The fate of these hydrous fluids depends on ambient physical and chemical conditions. Mostly they hydrate adjacent olivine grains in the chromitite or penetrate the surrounding dunite envelope. In some cases, the fluids dissolve into silicate melts to produce water-bearing clinopyroxene and/or hydrous minerals,

such as amphibole, or silicate and chromite grains that may later exsolve as clinopyroxene and magnetite lamellae. These investigations provide direct natural evidence for the presence and importance of water in the formation and evolution of chromite deposits, as inferred by earlier experimental studies.

Keywords: Podiform chromitite; Clinopyroxene; Olivine; Ophiolite; Water

1. Introduction

The discovery of various exotic minerals (e.g., diamond, moissanite) in podiform chromitites of ophiolites (e.g., Robinson et al., 2004; Yang et al., 2007) has led to a renewed interest in these enigmatic bodies and challenged many existing assumptions on the nature of the upper mantle and the extent of large-scale recycling of sub-oceanic lithosphere (e.g., Arai, 2013). The key to understanding the formation of podiform chromitites is to examine critically the nature and origin of their parental magmas. It is widely thought that high-Al and high-Cr chromitites are crystallized from MORB (mid-ocean ridge basalts) -type and boninite-type melts, respectively (e.g., Zhou et al., 1996; Pagé and Barnes, 2009). However, many details about podiform chromitite formation are still poorly understood in light of experimental and mineralogical data. For example, experiments show that chromite can form under dry conditions at temperatures of 1250 ±

100 °C and $f(O_2)$ around ±1 log units relative to the FMQ buffer (Irvine, 1977; Roeder and Reynolds, 1991), precluding the need for water. On the other hand, the common presence of hydrous inclusions (e.g., amphibole, phlogopite and fluids) in chromite (e.g., Melcher et al., 1997; Schiano et al., 1997; Borisova et al., 2012; González-Jiménez et al., 2014; Rollinson et al., 2018; Liu et al., 2018) is taken as evidence for the presence of hydrous fluids. Such hydrous inclusions may have been trapped contemporaneously with chromite crystallization or later during post-magmatic hydrothermal activity, e.g., during annealing and sintering processes that affect chromite in the presence of hydrous fluids (Lorand and Ceuleneer, 1989; Melcher et al., 1997; Johan et al., 2017; Kapsiotis et al., 2019). In addition, chromite in podiform chromitite typically undergoes sub-solidus re-equilibration with olivine making it difficult to determine parental melt compositions (e.g., Rollinson and Adetunji, 2015; Xiao et al., 2016; Zhang et al., 2019).

On the basis of experimental studies, Matveev and Ballhaus (2002) and Johan et al. (2017) suggest that water plays a major role in the crystallization and aggregation of chromite grains. However, as yet no clear, there is no direct natural evidence for the role of magmatic water or aqueous hydrothermal fluids in the formation of podiform chromitite in the mantle, nor has the fate of such water after chromitite formation been considered because of limited studies on water in natural samples (Yu et al., 2019). In this study, we

present new petrological and mineralogical data on ophiolitic chromitites and present direct measurements of water contents of clinopyroxene and olivine associated with chromite in these bodies. Using these data, we critically evaluate the origin of water in podiform chromitites and discuss the nature of their parental melts. We also consider the role played by interstitial water in the alteration of chromitites and their associated dunites.

2. Samples and analytical methods

A number of samples having chromite, olivine and clinopyroxene associations were collected from various ophiolites, including Kars in east Turkey, Lycian nappes in southwest Turkey, Kızıldağ and Pozantı-Karsantı in southeast Turkey, Kempirsai in Kazakhstan and Purang in western Tibet (Fig. 1). The petrographical and mineralogical features were carefully described as shown in Figs. 2-4 and Section 3. Major elements of clinopyroxenes in all these samples were analyzed, and trace elements of clinopyroxene associated with chromite in the Kızıldağ and Kars ophiolitic rocks were also measured. Larger-scale features of the ophiolites were taken from the literatures (e.g., Melcher et al., 1997; Saka et al., 2014; Chen et al., 2015, 2019; Su et al., 2015a, 2018, 2019; Avcı et al., 2017; Liu et al., 2018). Samples for water content analysis including mantle harzburgite, dunite and various types (disseminated, banded, anti-nodular, and massive) of chromitite,

were all collected from Kızıldağ ophiolite. The constituent minerals of the samples are very fresh (Fig. 2) and can be used for Fourier transform infrared spectrometry (FTIR).

Major element compositions of clinopyroxene associated with chromite in chromitite, dunite and harzburgite in the ophiolites were determined on thin sections using a JEOL JXA8100 electron probe microanalyser (EPMA) at the Institute of Geology and Geophysics, Chinese Academy of Sciences (IGGCAS). The analysis was conducted at the operating conditions of 5 μm beam diameter, 10 nA beam current, 15 kV accelerating voltage and 10-30 s counting time on peak. Natural and synthetic minerals were used for standard calibration, and a program based on the ZAF procedure was used for matrix corrections. The representative values are present in Table 1, and raw data are available in Supplementary Table S1.

Trace element concentrations of clinopyroxene were determined with a 193 nm Coherent COMPex Pro ArF Excimer laser coupled to an Agilent 7500a inductively coupled plasma mass spectrometer at IGGCAS. Before LA-ICP-MS analysis, thin sections previously coated with carbon for EPMA analyses were treated with 3% HNO_3, followed by de-ionized water and ethylene to clean the surfaces. Each analysis was performed using 80 μm-diameter ablating spots at 6 Hz with an energy of ~100 mJ per pulse for 45 s after measuring the gas blank for 20 s. Standard references materials NIST610 and NIST612

were used as external standards to produce calibration curves. Off-line data processing was performed using the GLITTER 4.0 program. The results are listed in Table 2.

Lithium concentration and isotopic ratio of clinopyroxene were measured using Cameca IMS 1280HR SIMS at IGGCAS. The O^- primary ion beam was accelerated at 13 kV, with an intensity of about 15 to 30 nA. The elliptical spot was approximately 20 × 30 μm in size. Positive secondary ions were measured on an ion multiplier in pulse counting mode, with a mass resolution (M/DM) of 1500 and an energy slit open at 40 eV without any energy offset. A 60-second pre-sputtering with raster was applied before analysis. The secondary ion beam position in apertures, as well as the magnetic field and the energy offset, were automatically centred before each measurement. Eighty cycles were measured with counting times of 7 and 2 seconds for ^6Li and ^7Li, respectively. The clinopyroxene standard 06JY29CPX (Su et al., 2015b) was used for calibration. The results are shown in Table 3.

Doubly-polished thin sections with a thickness ~0.2 mm were prepared for FTIR analysis. Unpolarized spectra were obtained from 1000 to 4500 cm^{-1} on a Nicolet iS50 FTIR coupled with a Continuum microscope in the School of Earth Sciences, Zhejiang University. The spectra were collected close to optically clean, inclusion- and crack-free areas of the grains. 128 scans were accumulated at a resolution of 4 cm^{-1}. A squared

aperture (30×30 to 100×100 μm^2) was used and adjusted depending on the mineral grain size and quality. More than 10 non-oriented grains of olivine and clinopyroxene in each section were measured under unpolarized light. Due to the absorbance of structural OH lower than 0.3, the water content calculated from average spectra in each section is reliable with a deviation of less than 10% (Withers, 2013). Water contents of minerals were calculated from FTIR spectra based on the Lambert-Beer law:

$$c=A/\varepsilon t\gamma$$

where c is the OH concentration (H_2O in wt. ppm), *A* is the integrated area (cm^{-2}) of absorption bands in the measured region, ε is the molar absorption coefficient ($ppm^{-1}\ cm^{-2}$), and t is the thickness of the sample (cm). The baseline was drawn by hand at least three times using the Nicolet Omnic software, and the uncertainty is less than 5%. The area of each analysis used to calculate the water content was averaged from three calculations. The thickness of the samples was measured using a digital micrometer and averaged from 20-30 measurements covering the whole section. Uncertainties in the calculated water contents come from: (1) using unpolarized infrared beams on unoriented minerals (<10%); (2) baseline correction (<5%); (3) variable sample thickness (<3%); and (4) differences between the absorption coefficients (<10%) of our samples and those of samples used by Bell et al. (1995) due to differences in composition. The total uncertainty is estimated to be

151 less than 20-30%. Detailed analytical methods and calculations were the same as described
152 in Xia et al. (2010). Average water contents of olivine, clinopyroxene and orthopyroxene in
153 the Kızıldağ ophiolitic rocks are shown in Table 4, and representative infrared spectrometry
154 spectra of olivine, clinopyroxene and orthopyroxene are illustrated in Fig. 3.
155

156 **3. Petrography**

157 **3.1. Clinopyroxene-bearing chromitite**

158 Silicate minerals associated with chromite in podiform chromitites are mainly olivine
159 (e.g., Borisova et al., 2012; Arai and Miura, 2016), but we show that podiform chromitites
160 in several Turkish ophiolites (Fig. 1) have a clinopyroxene matrix (Figs. 2, 4a-h). Such a
161 mineralogy is rare, having previously been reported only in the Celebration Mine, Oregon
162 (Thayer, 1969) and the Oman ophiolite (Rollinson and Adetunji, 2015). These chromitites
163 have textures ranging from massive, nodular and anti-nodular to banded and disseminated,
164 in order of decreasing abundance of chromite. Green clinopyroxene is visible in
165 hand-specimen (Fig. 2a) and occurs as anhedral crystals of variable size (Fig. 2b). It
166 occasionally coexists with olivine and orthopyroxene as silicate matrix of chromitite (Fig.
167 2c) or totally occupies the silicate matrix (Fig. 2d). Clinopyroxene in olivine-free chromitite
168 fills the interstices between chromite grains (Fig. 4a-c), whereas in olivine-bearing samples,

clinopyroxene is commonly present at the contacts between olivine and chromite grains, increasing abundance from the olivine to the chromite side (Fig. 4d-f). These clinopyroxene crystals, in most cases, are isolated by chromite grains with no external connections (Fig. 4b, c, f, h) and are even partly enclosed in some chromite grains (Fig. 4a) probably due to fast crystallization of chromite. The minerals are well preserved in most samples, and partly altered samples typically have more fresh relict grains (Fig. 4f-h) than the clinopyroxene-free varieties (Fig. 4).

The association of chromite and clinopyroxene is extensively developed in the associated dunite envelopes (Fig. 4i-m) and the host harzburgites of the Turkish ophiolites (Fig. 4n-p). In this association, chromite is commonly anhedral and is surrounded by clinopyroxene, which is morphologically distinct from the euhedral, interstitial grains (Fig. 4j). Clinopyroxene can form very thin films, partially or completely surrounding chromite grains, and in some cases, extending into cracks in olivine (Fig. 4k, l). Fresh olivine is present in almost equal quantities as the chromite and clinopyroxene, whereas in samples containing large chromite crystals with minor clinopyroxene, the olivine is serpentinized (Fig. 4m). Because ophiolitic harzburgite is a refractory rock, it typically contains very little clinopyroxene and rarely hosts chromite-clinopyroxene associations. However, in the Tethyan ophiolites, clinopyroxene occurs as intergrowths with chromite in the peridotites,

as interstitial grains surrounding chromite or surrounded by chromite (Fig. 4n-p). It is also noted that chromite grains associated with clinopyroxene are free of alteration, indicating no or less modification from later melt percolation. In summary, both the amount and grain size of clinopyroxene associated with chromite in ophiolitic rocks correlate positively with chromite abundance. The texture and mode of occurrence of the clinopyroxene grains, together with the compositions shown below, suggest that their crystallization were related with surface hydrous fluids (not necessarily aqueous fluids) between the chromite grains.

3.2. Selective alteration features in podiform chromitites

The former presence of hydrous fluids in ophiolitic podiform chromitites is also documented by the nature and distribution of alteration in these rocks. Podiform chromitites are normally surrounded by dunite envelopes, which grade outward into harzburgite (Fig. 5) (Lago et al., 1982). Alteration is common in chromitites, typically causing partial to complete replacement of olivine by serpentine (Fig. 5a), whereas the dunite envelopes and host harzburgites typically contain remnants of pristine olivine (Fig. 5b, c). The decreasing intensity of alteration outward from chromitite to dunite envelope to harzburgite clearly suggests that the hydrous fluids originated within the chromitite itself.

If the hydrous fluids responsible for alteration in chromitites came from external sources, the rocks would display a different pattern of alteration. Because dunite is less

205 competent than either chromitite or harzburgite, it can accommodate more stain than the
206 other lithologies (Rassios and Smith, 2000; Kapsiotis et al., 2019). Thus, as the temperature
207 decreases dunite may form brittle shear zones whereas the host harzburgite continues to
208 undergo ductile deformation (e.g., Boudier and Coleman, 1981; Zhang et al., 2019). Such
209 shear strain can cause tectonic thinning of the original dunite "envelope", facilitating fluid
210 penetration along the shear zones resulting in alteration of the dunite to even less competent
211 serpentinite (e.g., Boudier and Coleman, 1981; Rassios and Smith, 2000). If this process
212 occurs, intensity of alteration would decrease inward and the chromitite would be
213 surrounded by an envelope of serpentinite. This can explain why some chromitites, and
214 particularly their dunite envelopes, are more serpentinized than their host harzburgite. Thus,
215 the general increase in serpentinization outward from chromitite to dunite to harzburgite
216 indicates that the hydrous fluids responsible for the alteration likely originate from an
217 external source. It is opposite to the decreasing intensity of alteration outward from
218 chromitite to dunite envelope to harzburgite.

219 Selective alteration in banded chromitite ore (Fig. 5d) further suggests a close affinity
220 between fluids and chromite aggregates. Because chromite is a nominally anhydrous
221 mineral, the hydrous fluids producing the observed self-alteration presumably would have
222 been released from the surfaces of the chromite grains, which is thought to be coated with

223 water during crystallization (Matveev and Ballhaus, 2002).

224

225 **4. Mineral chemistry of chromitites**

226 **4.1. Chemistry of clinopyroxene associated with chromite**

227 The clinopyroxene compositions in our samples are essentially the same in the
228 different rock types (Fig. 6). All analyzed grains have relatively large variations in Na_2O
229 (<0.6 wt.%), Al_2O_3 (<4 wt.%) and Cr_2O_3 (0.2-1.7 wt.%). They are considerably richer in
230 SiO_2 (51-56 wt.%), Cr_2O_3 and CaO (21-26 wt.%), and more depleted in TiO_2 (<0.4 wt.%)
231 and FeO (<3 wt.%) than clinopyroxene from MORB and boninite (Fig. 6). Thus, they
232 appear to have crystallized from melts that were neither boninitic nor MORB-like in
233 composition.

234 Instead, the high Si and Ca, together with the low Fe and Al of the clinopyroxenes
235 (particularly those in the chromitites) suggest a possible relation with hydrothermal origin,
236 as in the Oman ophiolite (Python et al., 2007; Akizawa et al., 2011). Because the hydrous
237 fluids presumably were generated internally, they most likely were released from the
238 chromite surfaces. However, the composition may have been modified by chemical
239 exchange with chromite, akin to that between chromite and olivine (e.g., Pagé and Barnes,
240 2009; Xiao et al., 2016; Zhang et al., 2019). Such sub-solidus re-equilibration would have

241 produced Cr-enrichment and Fe-depletion in the clinopyroxene.

242 The identical trace element patterns of the clinopyroxenes in chromitite, harzburgite
243 and dunite (Fig. 7) further point to their cogenetic origin. They are featured by enrichments
244 of heavy rare earth elements (HREEs) and depletion of light rare earth elements (LREE),
245 which are comparable to the patterns of hydrothermal clinopyroxene (Fig. 7; Akizawa et al.,
246 2011). However, the overall higher trace element concentrations and remarkable negative
247 Ce, Sr, Ti and Y anomalies of the studied clinopyroxenes are far beyond the features of the
248 typical hydrothermal clinopyroxene. This suggests that the other component should have
249 involved during clinopyroxene formation. Such component could be inferred as evolved
250 melts from which olivine crystallized in the immiscible basalt-water system (Matveev and
251 Ballhaus, 2002).

252 The clinopyroxenes in chromitites has variable Li concentrations (0.29 to 2.52 ppm
253 with one up to 6.70 ppm) and δ^7Li values (-11.7 to 6.54 ‰ with one down to -29.9‰)
254 (Table 3). These results, together with Li isotopic compositions of olivines in chromitite,
255 exceed the normal ranges of MORB and arc lavas and extend to altered MORB, marine
256 sediment and eclogite (Fig. 8a), suggesting involvement of subduction components in the
257 parental melts from which olivine and clinopyroxene crystallized (Su et al., 2018; Chen et
258 al., 2019). The subduction components could be inferred as initial origin of water measured

259 in the study minerals.

260 **4.2. Water contents of olivine, clinopyroxene and orthopyroxene**

261 Olivine in harzburgite has no measurable water, which is consistent with its residual
262 origin. Two analyzed samples from dunite have relatively high H_2O contents of 13-38 ppm
263 (average of 24 ppm) and 17-70 ppm (average of 42 ppm) (Table 4), which are consistent
264 with their magmatic origins (Chen et al., 2015, 2019). The moderate H_2O content (4-13
265 ppm with average of 9 ppm) of olivine in a harzburgite-dunite transition sample indicates
266 minor water diffusion from dunite into harzburgite, which is consistent with fluid
267 infiltration outward into harzburgite as inferred above. Water content variation in
268 orthopyroxene between the rocks (harzburgite: 113 ppm; harzburgite-dunite transition: 59
269 ppm; chromitite: 74 ppm; Fig. 8b) likely reflects a mixed signature of partial melting and
270 diffusion.

271 Olivine in clinopyroxene-bearing chromitite has variable H_2O contents, with the
272 lowest values (9-25 ppm; average of 17 ppm) being in disseminated ore, and the highest (48
273 ppm and 53 ppm) in massive ore. Banded and anti-nodular ores contain olivine with
274 moderate H_2O contents with averages of 21 ppm and 24 ppm, respectively (Table 4).

275 In contrast, clinopyroxene grains in the massive ore have much higher H_2O contents
276 (average of 801 ppm) compared to the banded ore (366 ppm) (Table 4). These large water

This is a preprint, the final version is subject to change, of the American Mineralogist (MSA)
Cite as Authors (Year) Title. American Mineralogist, in press.
DOI: https://doi.org/10.2138/am-2020-7270

277 variations in olivine and clinopyroxene are not attributed to magmatic differentiation (e.g.,
278 Kohn and Grant, 2006), but are rather thought to be related to the different ore types. The
279 positive correlation between water content in silicate minerals and the modal abundance of
280 chromite (Figs. 3, 8b) implies that water in the silicate minerals was derived from hydrous
281 fluids on the chromite surfaces, supporting the conclusion that hydrous fluids are collected
282 on chromite during crystallization (Matveev and Ballhaus, 2002).
283

284 **5. Effects of hydrous fluids on chromite surfaces**

285 It has been experimentally documented that in immiscible basalt-water systems
286 chromite and olivine can be physically fractionated due to differential wetting properties of
287 fluid and melt on oxide and silicate surfaces; chromite collects exsolved fluid whereas
288 olivine does not (Ballhaus, 1998; Matveev and Ballhaus, 2002). As shown above some of
289 the hydrous fluids were trapped in clinopyroxene and olivine grains or mixed with evolving
290 melts to form large amounts of H_2O-rich clinopyroxene and hydrous minerals such as
291 amphibole. Excess hydrous fluids hydrate olivine in the chromitites and wall rocks (dunite
292 and harzburgite).

293 Such hydrous fluids could easily enhance chemical diffusion between silicate phases
294 and chromite (Shimizu and Okamoto, 2016; Bai et al., 2019). Some components in the

hydrous fluids might also be partitioned into olivine around chromite and even into chromite itself, which are later expelled in the form of mineral exsolutions (e.g., Liang et al., 2018). Such additional components in olivine of chromitite might also lead to some of the observed isotopic differences between olivine from dunite and chromitite (e.g., Li isotopes in Su et al., 2016, 2018). This may also partially explain the presence of clinopyroxene, chromite and magnetite lamellae in olivine (Xiong et al., 2017; Liang et al., 2018) and clinopyroxene and rutile lamellae in chromite (Yamamoto et al., 2009; Miura et al., 2012). Arai (2013) even suggested that hydrous mineral inclusions in chromite represent the actual origin of silicate lamellae. When conditions permit, clinopyroxene (Fig. 4; Rollinson and Adetunji, 2015) and amphibole (Melcher et al., 1997) could form by fluid-melt mixing. These minerals could accommodate most of the water in the fluids thus preventing hydration of the surrounding olivine. More recently, preiswerkite ($NaMg_2Al^{VI}Al^{IV}{}_2Si_2O_{10}(OH)_2$), found in chromitite of the Khoy ophiolite in Iran, has been interpreted as a precipitate from fluid trapped by chromite, which was possibly a precursor of the fluid (Zaeimnia et al., 2017).

From these observations, it is clear that surface hydrous fluids on chromite grains play a critical role in H_2O enrichment of associated olivine and clinopyroxene and such hydrous fluids may be responsible for the hydrous mineral inclusions commonly observed in

chromite grains. Additionally, such fluids might elevate $Fe^{3+}/\sum Fe$ ratios of chromite in chromitite making them unreliable for oxygen fugacity estimations (Melcher et al., 1997; Rollinson and Adetunji, 2015).

6. Implications: Initial origin and role of hydrous fluids in chromite deposit formation

On the basis of experimental data, water is considered to be a crucial phase controlling many aspects of chromite formation (Matveev and Ballhaus, 2002; Johan et al., 2017). For example, involvement of water in mafic magmas can lower the temperature of chromite crystallization, although the effect is less than for silicate minerals (Boudreau, 1999). The presence of water can also ensure that chromite is the first mineral to crystallize and can stabilize chromite on the liquidus of silicate melt (e.g., Lorand and Ceuleneer, 1989; Nicholson and Mathez, 1991). Our study provides petrographic, mineralogical and geochemical evidence confirming the occurrence and fate of water in podiform chromitites and inferring its direct origin from chromite grain surface and initial origin from subducting slab. We have shown that crystallizing chromite can collect water on its surface, which is the direct origin of hydrous fluids and may then hydrate surrounding grains of pyroxene and olivine. Matveev and Ballhaus (2002) suggest that very small, dispersed grains of chromite may even collect enough water to form bubbles. This allows chromite grains to

rise via decreasing density, thus promoting their gathering and concentration and enhancing melt-fluid immiscibility. The fate of the water in a podiform chromitite varies depending on local conditions. In most cases it hydrates surrounding silicate minerals in the chromitite and/or penetrates the surrounding wall rocks (Fig. 4). In some cases, it may mix with evolving melts to generate hydrothermal-like clinopyroxene (Fig. 2) or infiltrate silicates and chromite to form inclusions, which may exsolve later in the form of mineral lamella.

Matveev and Ballhaus (2002) estimated that for a basaltic melt to produce a chromite deposit it should have a high primary H_2O content (up to 4 wt.%), high enough to exsolve a water-rich fluid phase. Such high H_2O contents in mafic magmas are likely to exist only in supra-subduction zone (SSZ) environments. Lithium isotopic compositions of olivine and clinopyroxene in chromitites (Fig. 8a) confirm this inference. However, formation of chromite deposits is not exclusively related to the water contents of the host magmas. Such deposits can be hosted in Alaskan-type intrusions, and in SSZ-type and in MOR-like ophiolites. The host magmas for such deposits have highly variable water contents; e.g., 2.0-6.0 wt.% H_2O in island arc tholeiites (Plank et al., 2013; Ballhaus et al., 2015), 1.0-2.9 wt.% H_2O in boninites and 0.12-0.51 wt.% in MORB-like lavas (Sobolev and Chaussidon, 1996). The crystallization and accumulation of chromite in magmas with different water contents may reflect the pressure-dependent behavior of water (Keppler and

Bolfan-Casanova, 2006). At mantle or mantle-crust transition depths, where podiform chromitites commonly occur in ophiolites, hydrous minerals are rare in crystallizing magmas so whatever water is available to promote crystallization of chromite. Water can also be concentrated during magma-peridotite interaction (Arai et al., 1997), suggesting that economic deposits of chromitite may also form in relatively water-poor MORB systems. In this aspect, initial water content of the parental magmas is not critical for chromitite formation. We do not negate the widely accepted explanation of chromitite formation preferred in subduction settings, but do point out that on the grounds of efficiency, melt-fluid immiscibility should be of first importance.

Hydrous fluids tend to wet chromite much better than silicate phases (Matveev and Ballhaus, 2002), to an extent that chromite may be concentrated selectively in exsolved fluids when fluid saturation occurs at magmatic temperature. H_2O also depresses the liquidus temperatures of silicates more profoundly than that of chromite. A dry basaltic melt may be saturated with olivine and chromite, but the same melt at the same temperature will be chromite-only saturated if it contains a few percent of H_2O. Hence, podiform chromitites most readily form in hydrous basaltic to boninitic melts generated above intra-oceanic subduction zone.

Acknowledgements

This research was financially supported by the Second Tibetan Plateau Scientific Expedition and Research Program (STEP) (2019QZKK0801), National Natural Science Foundation of China (91755205 and 41772055) and the State Key Laboratory of Lithospheric Evolution (201701).

References

Ahmed, A.H., Arai, S. (2002). Unexpectedly high-PGE chromitite from the deeper mantle section of the northern Oman ophiolite and its tectonic implications. Contributions to Mineralogy and Petrology 143, 263-278.

Akizawa, N., Arai, S., Tamura, A., Uesugi, J., Python, M. (2011). Crustal diopsidites from the northern Oman ophiolite: evidence for hydrothermal circulation through suboceanic Moho. Journal of Mineralogical and Petrological Sciences 106, 261-266.

Anders, E., Grevesse, N. (1989). Abundances of the elements: meteoritic and solar. Geochimica et Cosmochimica Acta 53, 197-214.

Arai, S. (2013). Conversion of low-pressure chromitites to ultra-high-pressure chromitites by deep recycling: A good inference. Earth and Planetary Science Letters 379, 81-87.

Arai, S., Matsukage, K., Isobe, E., Vysotskiy, S. (1997). Concentration of incompatible elements in oceanic mantle: effect of melt/wall interaction in stagnant or failed conduits within peridotite. Geochimica et Cosmochimica Acta 61, 671-675.

Arai, S., Miura, M. (2016). Formation and modification of chromitites in the mantle. Lithos 264, 277-295.

Avcı, E., Uysal, I., Akmaz, R.M., Saka, S. (2017). Ophiolitic chromitites from the Kızılyüksek area of the Pozantı-Karsantı ophiolite (Adana, southern Turkey): Implication for crystallization from a fractionated boninitic melt. Ore Geology Reviews 90, 166-183.

Bai, Y., Su, B.X., Xiao, Y., Chen, C., Cui, M.M., He, X.Q., Qin, L.P., Charlier, B. (2019). Diffusion-driven chromium isotope fractionation in minerals of ultramafic cumulates: elemental and isotopic evidence from the Stillwater Complex. Geochimica et Cosmochimica Acta 263, 167-181.

Ballhaus, C. (1998). Origin of podiform chromite deposits by magma mingling. Earth and Planetary Science Letters 156, 185-193.

398 Ballhaus, C., Fonseca, R.I.O.C., Kirchenbaur, M., Zirner, A. (2015). Spheroidal textures in
399 igneous rocks–Textural consequences of H_2O saturation in basaltic melts. Geochimica
400 et Cosmochimica Acta 167, 241-252.Bell, D.R., Ihinger, P.D., Rossman, G.R. (1995).
401 Quantitative analysis of trace OH in garnet and pyroxenes. American Mineralogist 80,
402 465-474.
403 Borisova, A., Ceuleneer, G., Kamenetsky, V., Arai, S., Béjina, F., Bindeman, I., Polvé, M.,
404 de Parseval, P., Aigouy, T., Pokrovski, G. (2012). A new view on the petrogenesis of
405 the Oman ophiolite chromitites from microanalyses of chromite-hosted inclusions.
406 Journal of Petrology 53, 2411-2440.
407 Boudier, F., Coleman, R.G. (1981). Cross section through the peridotite in the Samail
408 ophiolite, southeastern Oman Mountains. Journal of Geophysical Research: Solid
409 Earth 86, 2573-2592.
410 Boudreau, A. (1999). Fluid fluxing of cumulates: the JM reef and associated rocks of the
411 Stillwater Complex, Montana. Journal of Petrology 40, 755-772.
412 Chen, C., Su, B.X., Uysal, I., Avcı, E., Zhang, P.F., Xiao, Y., He, Y.S. (2015). Iron isotopic
413 constraints on the origin of peridotite and chromitite in the Kızıldağ ophiolite,
414 southern Turkey. Chemical Geology 417, 115-124.
415 Chen, C., Su, B.X., Xiao, Y., Pang, K.N., Robinson, P.T., Uysal, İ., Lin, W., Qin, K.Z.,
416 Avcı, E., Kapsiotis A. (2019). Intermediate chromitite in Kızıldağ ophiolite (SE
417 Turkey) formed during subduction initiation in Neo-Tethys. Ore Geology Reviews
418 104, 88-100.
419 Dilek, Y., Furnes, H. (2009). Structure and geochemistry of Tethyan ophiolites and their
420 petrogenesis in subduction rollback systems. Lithos 113, 1-20.
421 González-Jiménez, J.M., Griffin, W.L., Proenza, J.A., Gervilla, F., O'Reilly, S.Y., Akbulut,
422 M., Pearson, N.J., Arai, S. (2014). Chromitites in ophiolites: How, where, when, why?
423 Part II. The crystallization of chromitites. Lithos 189, 140-158.
424 Irvine, T.N. (1977). Chromite crystallization in the join Mg_2SiO_4–$CaMgSi_2O_6$–
425 $CaAl_2Si_2O_8$–$MgCr_2O_4$–SiO_2. Carnegie Institution of Washington, Yearbook 76,
426 465-472.
427 Johan, Z., Martin, R.F., Ettler, V. (2017). Fluids are bound to be involved in the formation
428 of ophiolitic chromite deposits. European Journal of Mineralogy 29, 543-555.

Kapsiotis, A., Economou-Eliopoulos, M., Zheng, H., Su, B.X., Lenaz, D., Jing, J.J., Antonelou, A., Velicogna, M., Xia, B. (2019). Refractory chromitites recovered from the Eretria mine, East Othris massif (Greece): Implications for metallogeny and deformation of chromitites within the lithospheric mantle portion of a forearc-type ophiolite. Geochemistry 79, 130-152.

Keppler, H., Bolfan-Casanova, N. (2006). Thermodynamics of water solubility and partitioning. Reviews in Mineralogy and Geochemistry 62, 193-230.

Kohn, S.C., Grant, K.J. (2006). The partitioning of water between nominally anhydrous minerals and silicate melts. Reviews in Mineralogy and Geochemistry 62, 231-241.

Lago, B.L., Rabinowicz, M., Nicolas, A. (1982). Podiform chromitite ore bodies: a genetic model. Journal of Petrology 23, 103-125.

Liang, Z., Xiao, Y., Thakurta, J., Su, B.X., Chen, C., Bai, Y., Sakyi, P.A., 2018. Exsolution lamellae in olivine grains of dunite units from different types of mafic-utramafic complexes. Acta Geologica Sinica 92, 586-599.

Liu, X., Su, B.X., Bai, Y., Chen, C., Xiao, Y., Liang, Z., Yang, S.H., Peng, Q.S., Su, B.C., Liu, B. (2018). Ca-enrichment characteristics of parental magmas of chromitite in ophiolite: inference from mineral inclusions. Earth Science 43, 1038-1050 (in Chinese with English abstract).

Lorand, J.P., Ceuleneer, G. (1989). Silicate and base-metal sulfide inclusions in chromites from the Maqsad area (Oman ophiolite, Gulf of Oman): a model for entrapment. Lithos 22, 173-190.

Matveev, S., Ballhaus, C. (2002). Role of water in the origin of podiform chromitite deposits. Earth and Planetary Science Letters 203, 235-243.

Melcher, F., Grum, W., Simon, G., Thalhammer, T.V., Stumpfl, E.F. (1997). Petrogenesis of the ophiolitic giant chromite deposits of Kempirsai, Kazakhstan: a study of solid and fluid inclusions in chromite. Journal of Petrology 38, 1419-1458.

Miura, M., Arai, S., Ahmed, A.H., Mizukami, M., Okuno, M., Yamamoto, S. (2012). Podiform chromitite classification revisited: a comparison of discordant and concordant chromitite pods from Wadi Hilti, northern Oman ophiolite. Journal of Asian Earth Sciences 59, 52-61.

459 Nicholson, D.M., Mathez, E.A. (1991). Petrogenesis of the Merensky Reef in the
460 Rustenburg section of the Bushveld Complex. Contributions to Mineralogy and
461 Petrology 107, 293-309.
462 Pagé, P., Barnes, S.J. (2009). Using trace elements in chromites to constrain the origin of
463 podiform chromitites in the Thetford Mines ophiolite, Québec, Canada. Economic
464 Geology 104, 997-1018.
465 Plank, T., Kelley, K.A., Zimmer, M.M., Hauri, E.H., Wallace, P.J. (2013). Why do mafic
466 arc magmas contain ~4 wt% water on average? Earth and Planetary Science Letters
467 364, 168-179.
468 Python, M., Ceuleneer, G., Ishida, Y., Barrat, J.A., Arai, S. (2007). Oman diopsidites: a
469 new lithology diagnostic of very high temperature hydrothermal circulation in mantle
470 peridotite below oceanic spreading centres. Earth and Planetary Science Letters 255,
471 289-305.
472 Rassios, A., Smith, A.G. (2000). Constraints on the formation and emplacement age of
473 western Greek ophiolites (Vourinos, Pindos, and Othris) inferred from deformation
474 structures in peridotites. Special Papers-Geological Society of America 473-484.
475 Robinson, P.T., Bai, W.J., Malpas, J., Yang, J.S., Zhou, M.F., Fang, Q.S., Hu, X.F.,
476 Cameron, S., Staudigel, H. (2004). Ultra-high pressure minerals in the Luobusa
477 ophiolite, Tibet, and their tectonic implications. Geological Society London Special
478 Publication 226, 247-271.
479 Roeder, P.L., Reynolds, I. (1991). Crystallization of chromite and chromium solubility in
480 basaltic melts. Journal of Petrology 32, 909-934.
481 Rollinson, H., Adetunji, J. (2015). The geochemistry and oxidation state of podiform
482 chromitites from the mantle section of the Oman ophiolite: a review. Gondwana
483 Research 27, 543-554.
484 Rollinson, H., Mameri, L., Barry, T. (2018). Polymineralic inclusions in mantle chromitites
485 from the Oman ophiolite indicate a highly magnesian parental melt. Lithos 310-311,
486 381-391.
487 Saka, S., Uysal, I., Akmaz, R.M., Kaliwoda, M., Hochleitner, R. (2014). The effects of
488 partial melting, melt-mantle interaction and fractionation on ophiolite generation:

489 constraints from the Late Cretaceous Pozanti-Karsanti Ophiolite, southern Turkey.
490 Lithos 202-203, 300-316.
491 Schiano, P., Clocchiatti, R., Lorand, J.P., Massare, D., Deloule, E., Chaussidon, M. (1997).
492 Primitive basaltic melts included in podiform chromites from the Oman ophiolite.
493 Earth and Planetary Science Letters 146, 489-497.
494 Shimizu, H., Okamoto, A. (2016). The roles of fluid transport and surface reaction in
495 reaction-induced fracturing, with implications for the development of mesh textures in
496 serpentinites. Contributions to Mineralogy and Petrology 171, 73.
497 Sobolev, A.V., Chaussidon, M. (1996). H_2O concentrations in primary melts from
498 supra-subduction zones and mid-ocean ridges: implications for H_2O storage and
499 recycling in the mantle. Earth and Planetary Science Letters 137, 45-55.
500 Su, B.X., Chen, C., Pang, K.N., Sakyi, P.A., Uysal, I., Avcı, E., Zhang, P.F. (2018). Melt
501 penetration in oceanic lithosphere: Li isotope records from the Pozantı-Karsantı
502 ophiolite in southern Turkey. Journal of Petrology 59, 191-205.
503 Su, B.X., Teng, F.Z., Hu, Y., Shi, R.D., Zhou, M.F., Zhu, B., Liu, F., Gong, X.H., Huang,
504 Q.S., Xiao, Y., Chen, C., He, Y.S. (2015a). Iron and magnesium isotope fractionation
505 in oceanic lithosphere and sub-arc mantle: perspectives from ophiolites. Earth and
506 Planetary Science Letters 430, 523-532.
507 Su, B.X., Gu, X.Y., Deloule, E., Zhang, H.F., Li, Q.L., Li, X.H., Vigier, N., Tang, Y.J.,
508 Tang, G.Q., Liu, Y., Brewer, A., Mao, Q., Ma, Y.G. (2015b). Potential orthopyroxene,
509 clinopyroxene and olivine reference materials for in situ lithium isotope determination.
510 Geostandards and Geoanalytical Research 39, 357-369.Su, B.X., Zhou, M.F., Jing, J.J.,
511 Robinson, P.T., Chen, C., Xiao, Y., Liu, X., Shi, R.D., Lenaz, D., Hu, Y. (2019).
512 Distinctive melt activity and chromite mineralization in Luobusa and Purang
513 ophiolites, southern Tibet: constraints from trace element compositions of chromite
514 and olivine. Science Bulletin 64, 108-121.
515 Su, B.X., Zhou, M.F., Robinson, P.T. (2016). Extremely large fractionation of Li isotopes
516 in chromitite-bearing mantle sequence. Scientific Reports 6, 22370.
517 Thayer, T.P. (1969). Gravity differentiation and magmatic re-emplacement of podiform
518 chromite deposits. Economic Geology Monograph 4, 132-146.

519 Tomascak, P.B., Magna, T., Dohmen, R. (2016). Advances in Lithium Isotope
520 Geochemistry. Berlin: Springer.
521 Withers, A.C. (2013). On the use of unpolarized infrared spectroscopy for quantitative
522 analysis of absorbing species in birefringent crystals. American Mineralogist 98,
523 689-697.
524 Xia, Q.K., Hao, Y., Li, P., Deloule, E., Coltorti, M., Dallai, L., Yang, X., Feng, M. (2010).
525 Low water content of the Cenozoic lithospheric mantle beneath the eastern part of the
526 North China Craton. Journal of Geophysical Research: Solid Earth 115(B7).
527 Xiao, Y., Teng, F.Z., Su, B.X., Hu, Y., Zhou, M.F., Zhu, B., Shi, R.D., Huang, Q.S., Gong,
528 X.H., He, Y.S. (2016). Iron and magnesium isotopic constraints on the origin of
529 chemical heterogeneity in podiform chromitite from the Luobusa ophiolite, Tibet.
530 Geochemistry, Geophysics, Geosystems 17, 940-953.
531 Xiong, F., Yang, J., Dilek, Y., Wang, C. (2017). Nanoscale diopside and spinel exsolution
532 in olivine from dunite of the Tethyan ophiolites, southwestern Turkey: Implications
533 for the multi-stage process. Journal of Nanoscience and Nanotechnology 17,
534 6587-6596.
535 Yamamoto, S., Komiya, T., Hirose, K., Maruyama, S. (2009). Coesite and clinopyroxene
536 exsolution lamellae in chromites: in-situ ultrahigh-pressure evidence from podiform
537 chromitites in the Luobusa ophiolite, southern Tibet. Lithos 109, 314-322.
538 Yang, J.S., Dobrzhinetskaya, L., Bai, W.J., Fang, Q.S., Robinson, P.T., Zhang, J., Green,
539 H.W. (2007). Diamond-and coesite-bearing chromitites from the Luobusa ophiolite,
540 Tibet. Geology 35, 875-878.
541 Yu, M., Wang, Q., Yang, J.S. (2019). Fabrics and water contents of peridotites in the
542 Neotethyan Luobusa ophiolite, Southern Tibet: Implications for mantle recycling in
543 supra-subduction zones. Journal of the Geological Society176, 975-991.
544 Zaeimnia, F., Arai, S., Mirmohammadi, M. (2017). Na-rich character of
545 metasomatic/metamorphic fluids inferred from preiswerkite in chromitite pods of the
546 Khoy ophiolite in Iran: Role of chromitites as capsules of trapped fluids. Lithos
547 268-271, 351-363.
548 Zhang, P.F., Zhou, M.F., Liu, Q.Y., Malpas, J., Robinson, P.T., He, Y.S. (2019).
549 Modification of mantle rocks by plastic flow below spreading centers: Fe isotopic and

fabric evidence from the Luobusa ophiolite, Tibet. Geochimica et Cosmochimica Acta 253, 84-110.

Zhou, M.F., Robinson, P.T., Malpas, J., Li, Z. (1996). Podiform chromitites from the Luobusa ophiolite (southern Tibet): implications for melt-rock interaction and chromite segregation. Journal of Petrology 37, 3-21.

Figure captions:

Fig. 1. Distribution of the Tethyan ophiolites and highlighted locations of the studied ophiolites including Lyclan nappes, Pozantı-Karsantı, Kızıldağ, Kars, Kempirsai and Purang (modified after Dilek and Furnes, 2009).

Fig. 2. Clinopyroxene occurrence in hand-specimen (a), thin-section (b) and microphotographs (c, d) of chromitites from the Kızıldağ ophiolite.

Fig. 3. Representative infrared spectrometry spectra of olivine (a), clinopyroxene (b) and orthopyroxene (c) in harzburgite, dunite and various chromitite of the Kızıldağ ophiolite.

Fig. 4. Features of chromite-clinopyroxene association in a variety of rocks from several ophiolites. a, b) Disseminated and massive chromitite (Cic15-10) from Kars ophiolite; c) Massive chromitite (PK14-02) from Pozantı-Karsantı ophiolite; d) Massive chromitite (KZ15-21), e) Nodular chromitite (KZ15-31), f) Anti-nodular chromitite (KZ15-23), and g) Banded chromitite (KZ14-32-01) from Kızıldağ ophiolite; h) Disseminated chromitite (LN15-05) from Lycian nappes ophiolite; i) Dunite (PL14-3-1), j) Dunite (PL14-5-10), k) Dunite (PL14-5-12) from Purang ophiolite; l) Dunite (KZ15-16) from Kızıldağ ophiolite; m) Dunite (PK14-70) from Pozantı-Karsantı ophiolite; n) Harzburgite (PK14-35) from Pozantı-Karsantı ophiolite; o) Harzburgite (KZ14-24) from Kızıldağ ophiolite; p) Lherzolite (PL14-5-7) from Purang ophiolite. Chr, chromite; Cpx, clinopyroxene; Opx, orthopyroxene; Ol, olivine; Srp, serpentine.

Fig. 5. General features of podiform chromitite in ophiolites showing chromitite enveloped by dunite with a serpentine corona between them. a) Olivine in chromitite is almost entirely serpentinized with rare relicts; b) A few partly altered olivine grains are preserved in the serpentine corona; c) Less-altered olivine grains are present in the dunite; d) Banded chromitite (PK14-52) from the Pozantı-Karsantı ophiolite showing narrow bands of serpentine between olivine and chromite bands.

Fig. 6. Compositions (wt.%) of clinopyroxene associated with chromite in chromitite, dunite and harzburgite of ophiolites compared to those in boninites and mid-ocean ridge basalts (MORBs) (GEOROC database) and hydrothermal clinopyroxene (Akizawa et al., 2011).

Fig. 7. Chondrite-normalized rare earth element and primitive mantle-normalized trace element patterns of clinopyroxene associated with chromite in the Kızıldağ ophiolitic rocks. Hydrothermal clinopyroxene data are from Akizawa et al. (2011) and chondrite normalizing values from Anders and Grevesse (1989).

Fig. 8. (a) Correlation diagram of δ^7Li and 1/Li of clinopyroxene in the Kızıldağ chromitites with comparison of those published values in olivine (Chen et al., 2019) and (b) H_2O content variations of minerals from harzburgite to dunite and chromitite. The δ^7Li ranges of MORB, arc lava, eclogite, altered MORB and marine sediment are from Tomascak et al. (2016) and references therein.

Tables:

Table 1 Representative data of major element contents of clinopyroxene associated with chromite in chromitites and peridotites from ophiolites.

Table 2 Trace elemental compositions of clinopyroxene associated with chromite in chromitites and peridotites from ophiolites.

Table 3 Li isotopic compositions of clinopyroxene in Kizildag chromitites.

Table 4 H_2O contents of olivine, clinopyroxene and orthopyroxene in the rocks from the Kızıldağ ophiolite.

This is a preprint, the final version is subject to change, of the American Mineralogist (MSA)
Cite as Authors (Year) Title. American Mineralogist, in press.
DOI: https://doi.org/10.2138/am-2020-7270

Fig. 1

This is a preprint, the final version is subject to change, of the American Mineralogist (MSA)
Cite as Authors (Year) Title. American Mineralogist, in press.
DOI: https://doi.org/10.2138/am-2020-7270

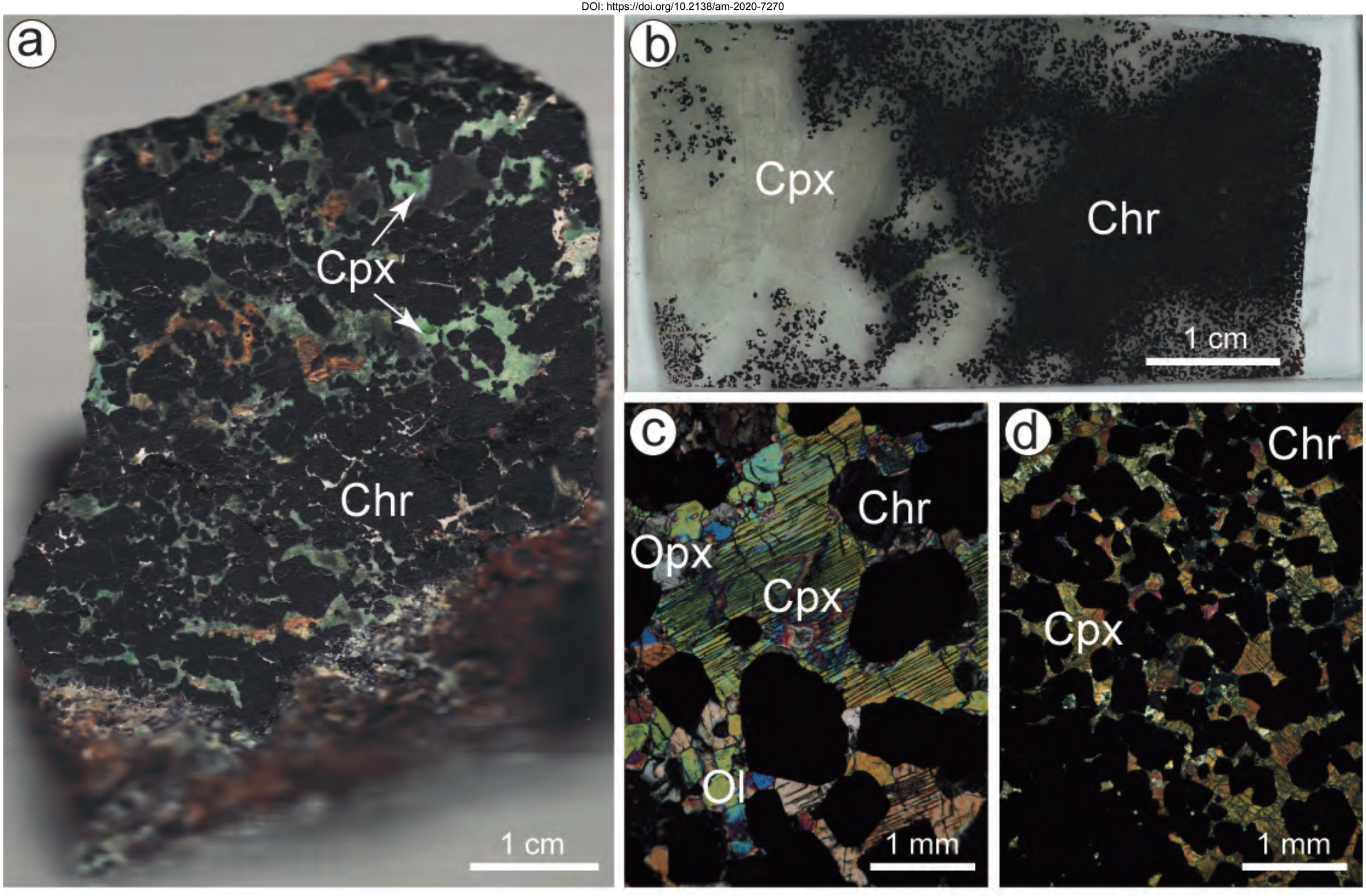

Fig. 2

This is a preprint, the final version is subject to change, of the American Mineralogist (MSA)
Cite as Authors (Year) Title. American Mineralogist, in press.
DOI: https://doi.org/10.2138/am-2020-7270

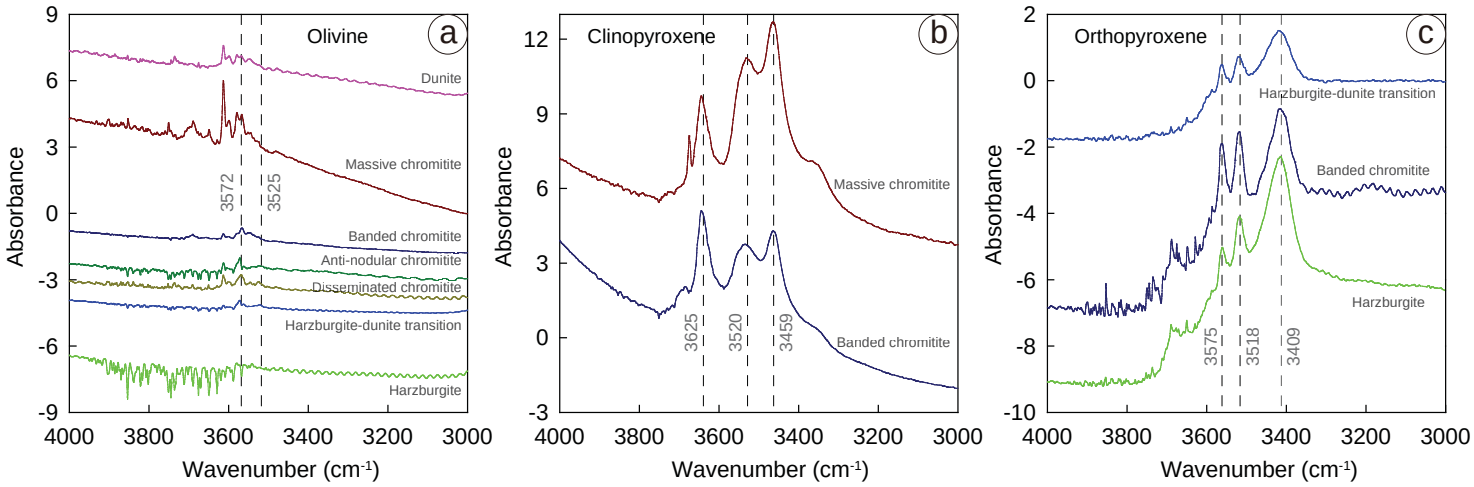

Fig. 3

This is a preprint, the final version is subject to change, of the American Mineralogist (MSA)
Cite as Authors (Year) Title. American Mineralogist, in press.
DOI: https://doi.org/10.2138/am-2020-7270

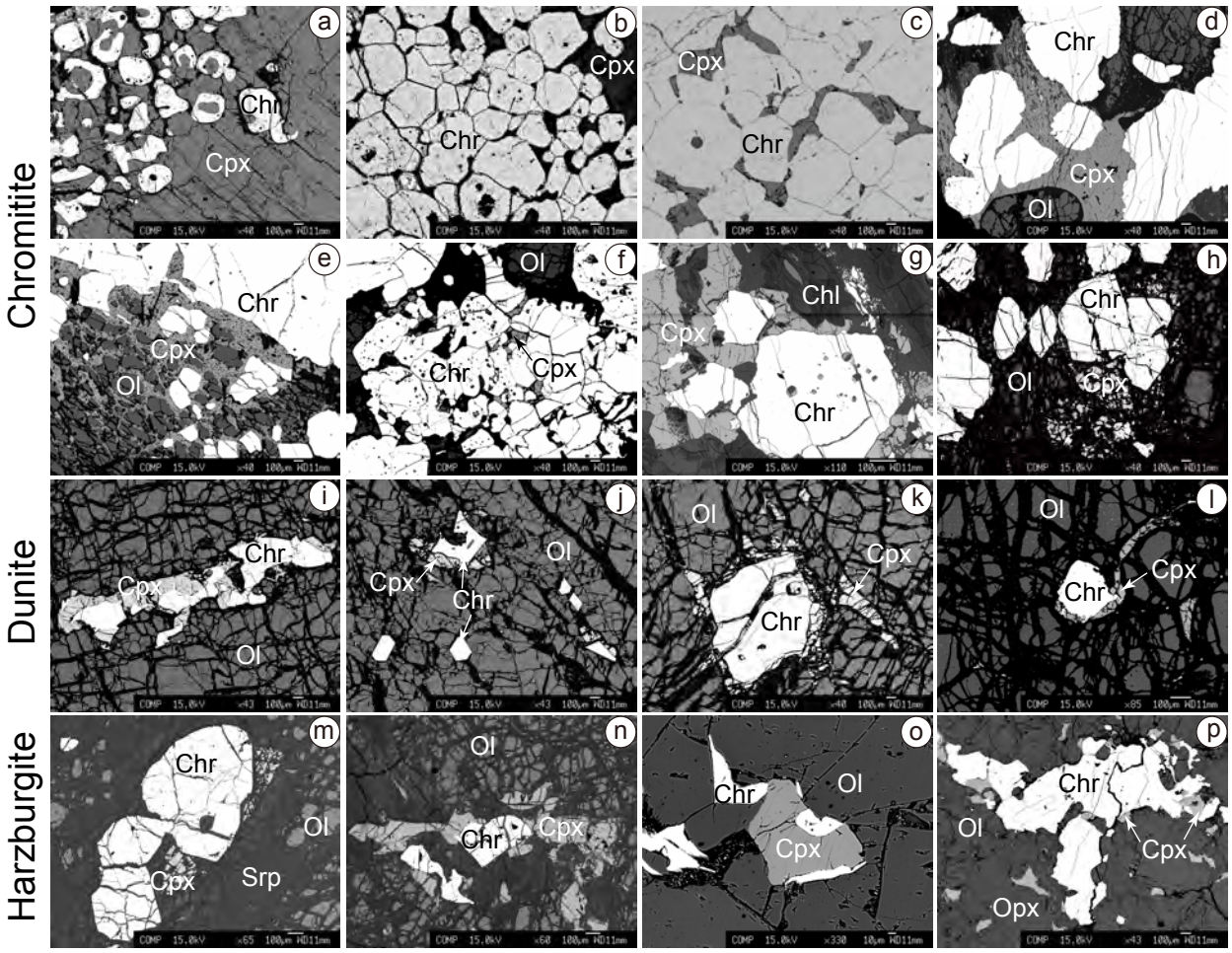

Fig. 4

This is a preprint, the final version is subject to change, of the American Mineralogist (MSA)
Cite as Authors (Year) Title. American Mineralogist, in press.
DOI: https://doi.org/10.2138/am-2020-7270

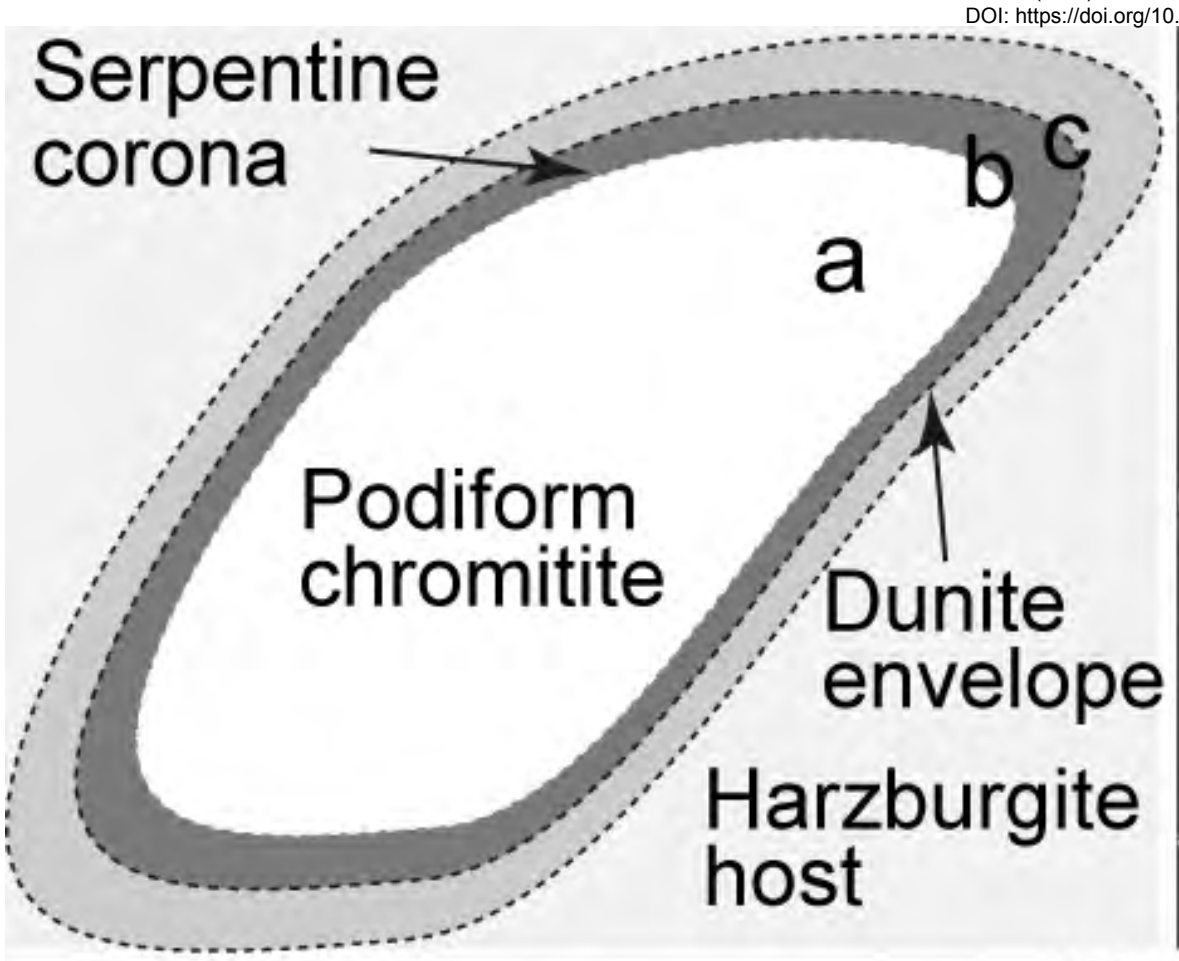

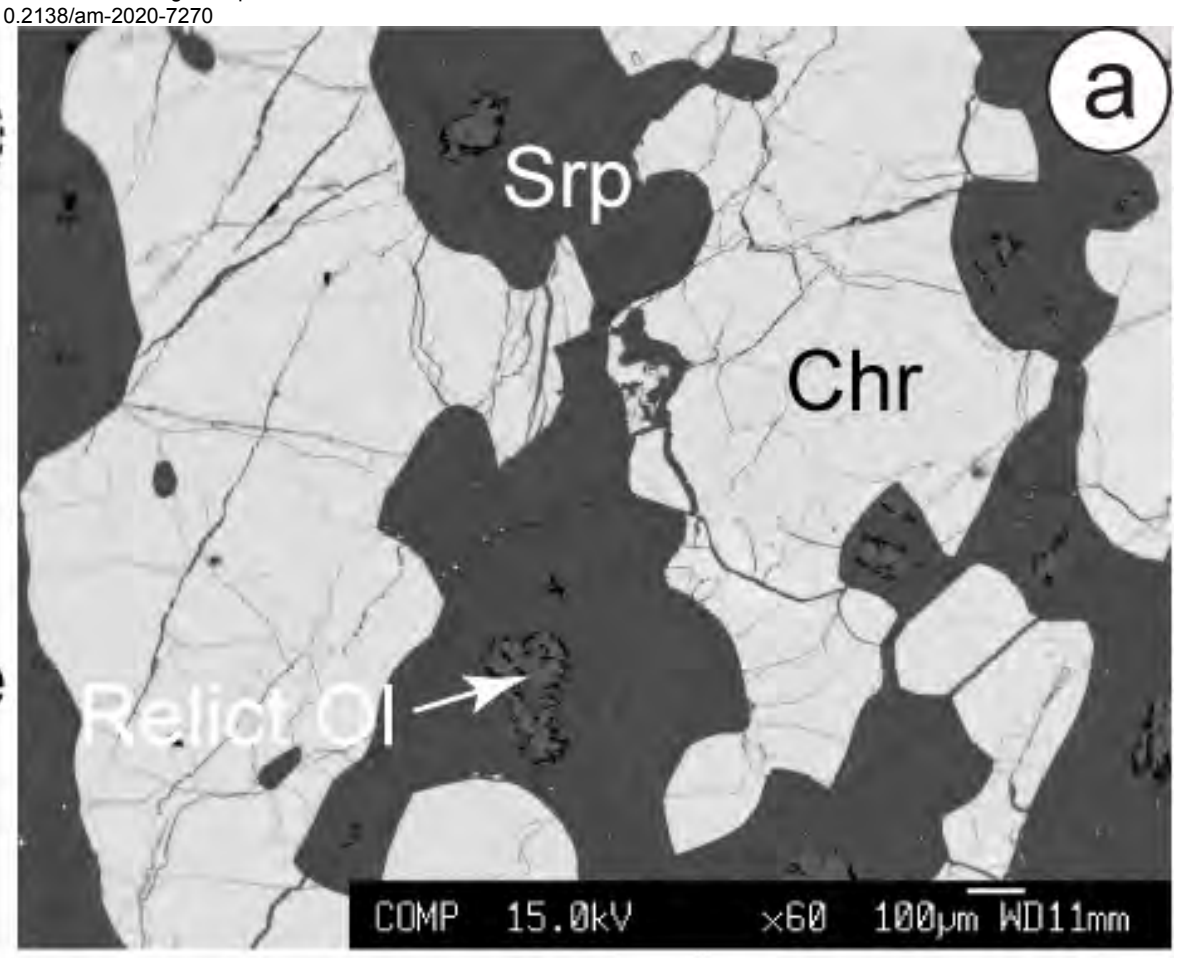

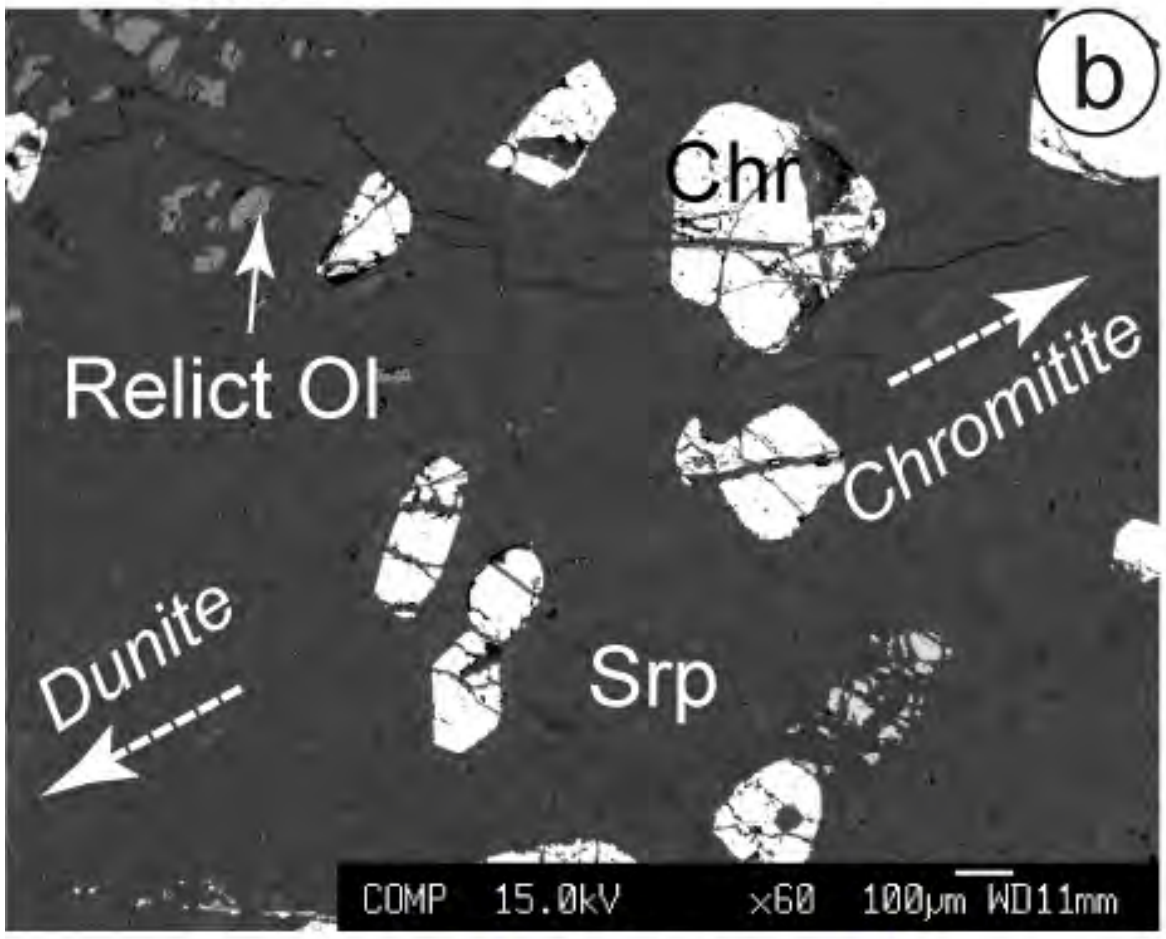

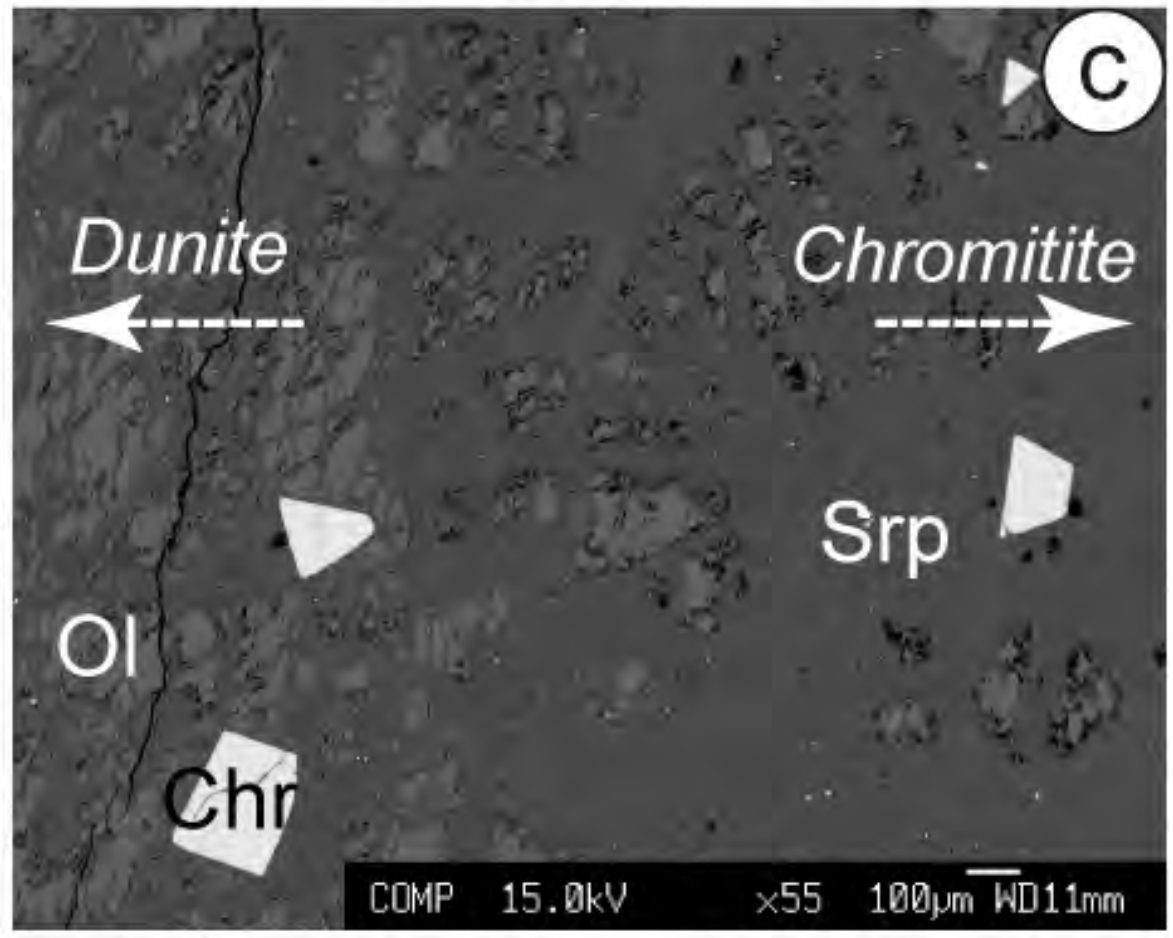

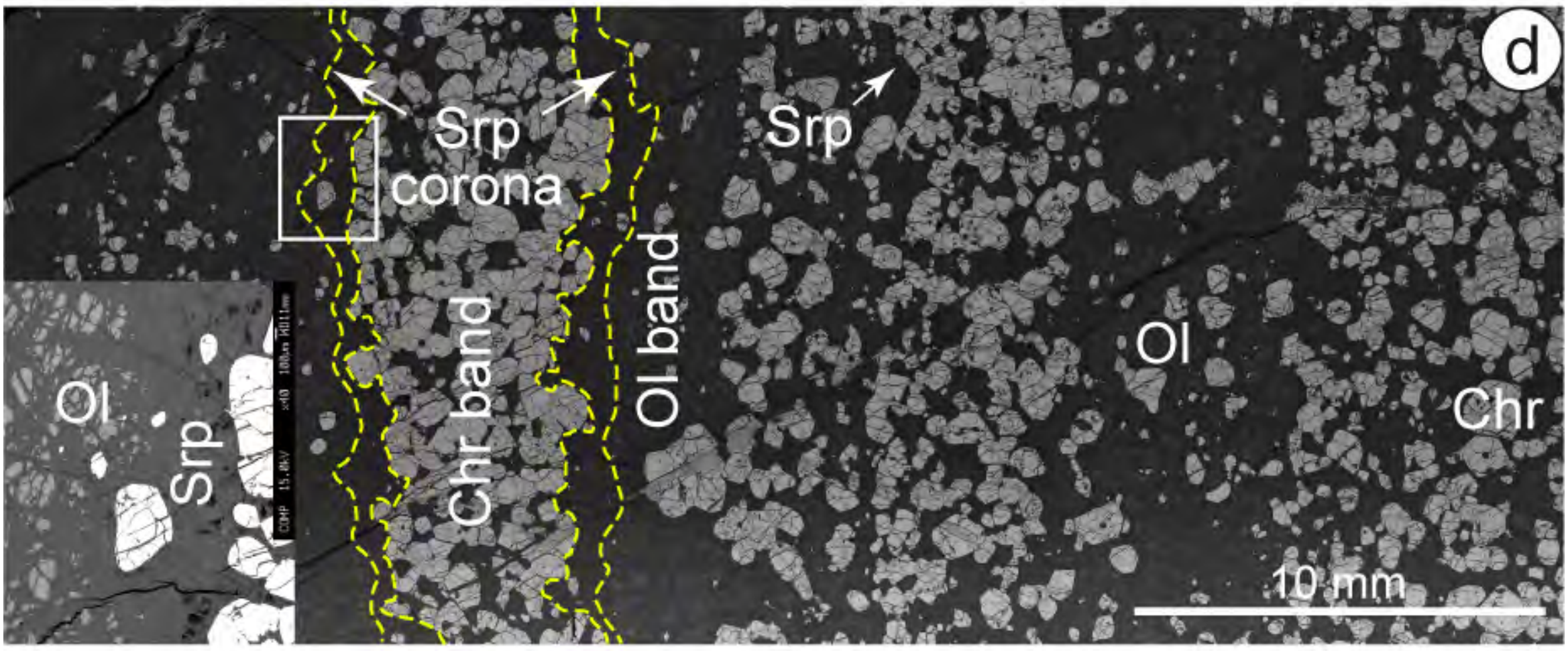

Fig. 5

This is a preprint, the final version is subject to change, of the American Mineralogist (MSA)
Cite as Authors (Year) Title. American Mineralogist, in press.
DOI: https://doi.org/10.2138/am-2020-7270

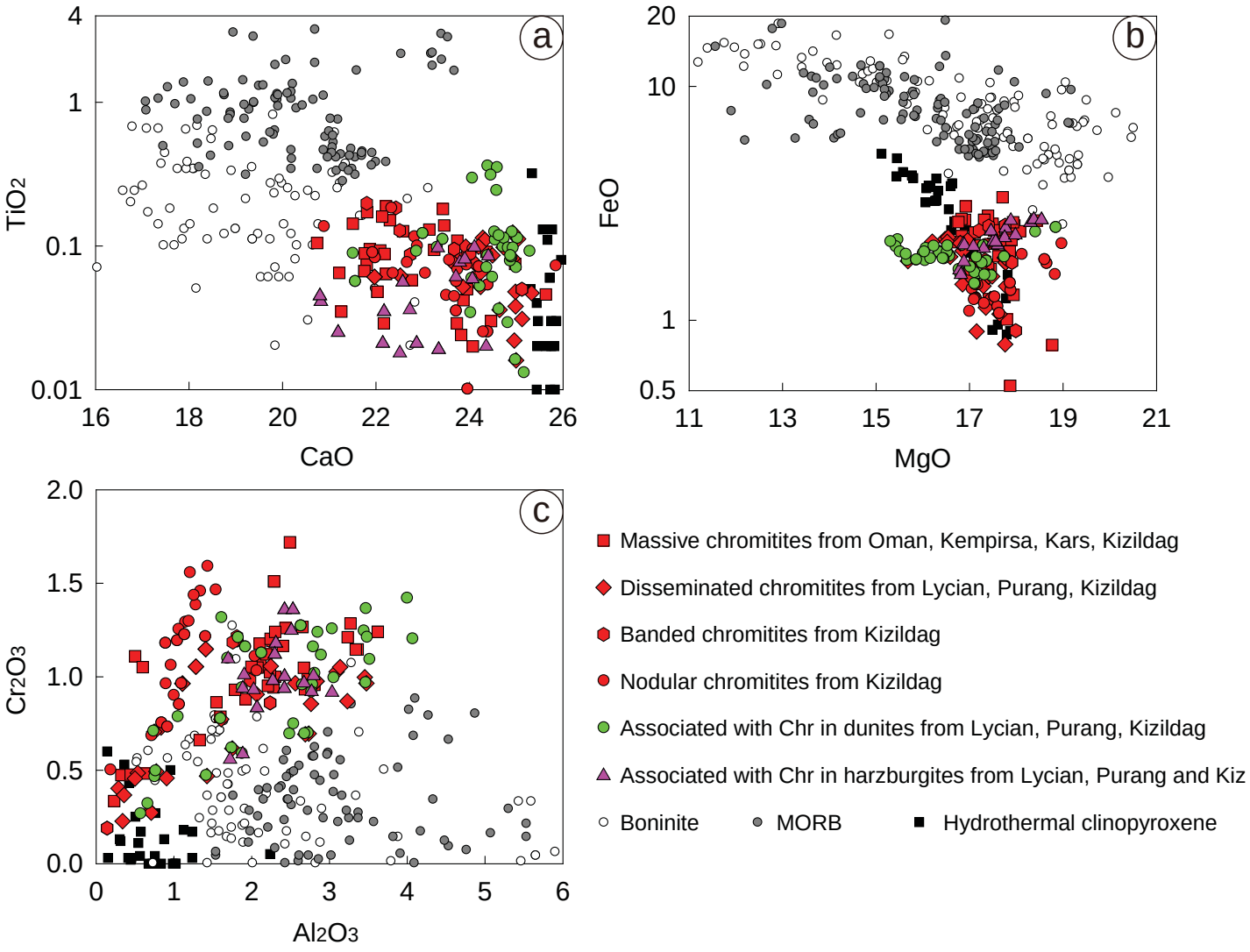

Fig. 6

This is a preprint, the final version is subject to change, of the American Mineralogist (MSA)
Cite as Authors (Year) Title. American Mineralogist, in press.
DOI: https://doi.org/10.2138/am-2020-7270

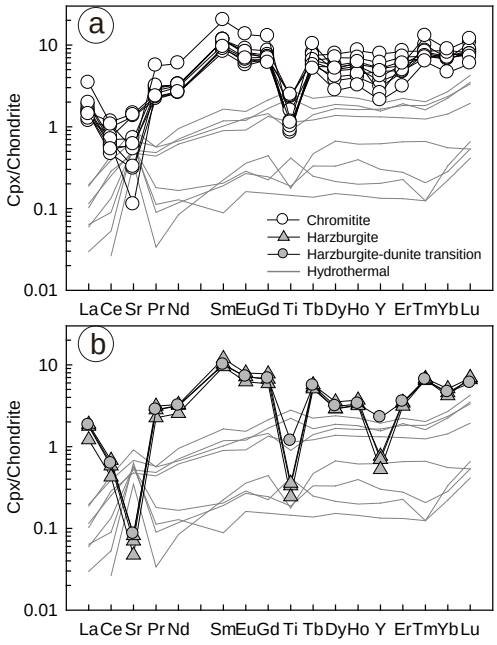

Fig. 7

This is a preprint, the final version is subject to change, of the American Mineralogist (MSA)
Cite as Authors (Year) Title. American Mineralogist, in press.
DOI: https://doi.org/10.2138/am-2020-7270

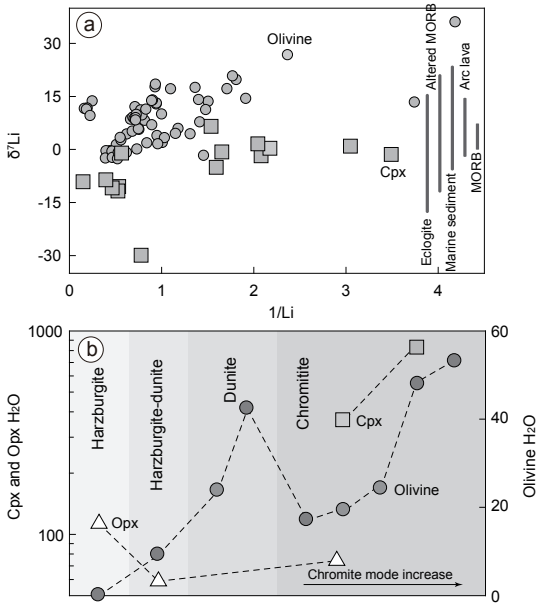

Fig. 8

This is a preprint, the final version is subject to change, of the American Mineralogist (MSA)
Cite as Authors (Year) Title. American Mineralogist, in press.
DOI: https://doi.org/10.2138/am-2020-7270

Table 1. Representative data of major element contents of clinopyroxene in associated with chromite in chromitites and peridotites from ophiolites.

Sample	Rock type	No.	SiO_2	TiO_2	Al_2O_3	Cr_2O_3	FeO	MnO	MgO	CaO	Na_2O	K_2O	NiO	Total	Mg#
Oman															
61*	Massive chromitite	1	52.5	0.02	2.30	1.00	1.74	0.11	17.1	24.1	0.18	0.05		99.1	94.7
Kempirsai, Kazakhstan															
AZ1B**	Chromitite	1	56.5	0.03	0.50	1.11	0.78	0.10	18.8	24.5	0.08	0.03	0.12	102.5	97.7
Kars, Turkey															
Cic15-10	Massive chromitite	10	53.9	0.09	1.97	0.78	2.59	0.12	17.3	22.9	0.19	0.00	0.06	99.9	92.3
Cic15-13	Massive chromitite	6	55.4	0.06	0.96	0.35	2.39	0.08	17.3	24.0	0.08	0.02	0.04	100.7	92.9
Lycian nappes, Turkey															
LN15-05	Sparsely disseminated chromitite	3	55.0	0.04	0.54	0.49	0.89	0.02	17.2	25.0	0.17	0.01	0.03	99.3	97.2
LN15-06	Sparsely disseminated chromitite	5	54.8	0.05	0.29	0.40	1.23	0.01	17.5	25.0	0.12	0.00	0.07	99.5	96.2
LN15-13	Sparsely disseminated chromitite	3	54.0	0.01	0.91	0.46	1.42	0.07	16.8	25.2	0.09	0.00	0.07	99.1	95.5
LN15-15	Dunite	3	54.5	0.03	0.76	0.46	1.42	0.00	17.1	24.8	0.14	0.00	0.01	99.3	95.6
LN15-18	Harzburgite	3	53.6	0.06	1.70	1.10	1.63	0.01	16.8	24.1	0.10	0.00	0.04	99.1	94.9
Kızıldağ, Turkey															
KZ14-17	Disseminated chromitite	1	54.3	0.07	0.84	0.73	1.40	0.04	17.3	24.2	0.18	0.00	0.02	99.1	95.7
KZ15-10	Disseminated chromitite	8	53.2	0.05	3.45	1.00	2.22	0.02	16.5	23.9	0.07	0.00	0.06	100.4	93.0
KZ14-20	Disseminated chromitite	4	53.6	0.06	1.28	1.05	1.84	0.06	17.8	22.0	0.58	0.00	0.06	98.2	94.6
KZ15-24	Disseminated chromitite	2	53.7	0.08	1.11	0.96	1.53	0.00	17.4	24.1	0.24	0.02	0.09	99.3	95.3
KZ14-32-1	Banded chromitite	4	53.6	0.10	1.81	1.20	1.76	0.00	17.9	23.7	0.16	0.01	0.05	100.3	94.8
KZ14-27-2	Banded chromitite	6	46.8	2.06	10.6	2.69	3.06	0.05	18.8	11.1	2.97	0.14	0.09	98.4	91.7
KZ15-27	Nodular chromitite	4	53.8	0.03	0.85	0.75	1.33	0.00	17.9	24.4	0.31	0.01	0.08	99.4	96.0
KZ15-37	Nodular chromitite	7	54.0	0.07	1.22	1.55	1.24	0.00	17.1	23.8	0.40	0.01	0.10	99.6	96.1
KZ15-32	Nodular chromitite	2	53.8	0.10	1.44	1.59	1.62	0.03	17.0	22.9	0.32	0.01	0.02	98.8	95.0
KZ15-29	Nodular-disseminated chromitite	5	54.8	0.03	0.91	0.96	1.24	0.04	17.5	24.3	0.27	0.00	0.05	100	96.2
KZ15-31	Nodular chromitite	14	55.3	0.07	0.20	0.50	0.34	0.00	17.7	25.9	0.03	0.00	0.05	100	98.9
KZ14-32-2	Massive chromitite	12	54.4	0.19	2.11	1.07	2.22	0.05	17.8	22.2	0.39	0.00	0.02	100	93.5
KZ15-38	Massive chromitite	6	54.2	0.08	1.33	0.66	2.08	0.12	17.2	23.7	0.18	0.00	0.06	99.6	93.7

This is a preprint, the final version is subject to change, of the American Mineralogist (MSA)
Cite as Authors (Year) Title. American Mineralogist, in press.
DOI: https://doi.org/10.2138/am-2020-7270

KZ15-25	Massive chromitite	4	53.4	0.04	2.43	1.26	2.39	0.05	18.1	21.3	0.28	0.00	0.06	99.3	93.1
KZ14-38	Massive chromitite	2	53.2	0.07	2.29	1.51	1.96	0.00	17.9	21.8	0.40	0.01	0.09	99.2	94.3
KZ15-21	Massive chromitite	5	51.9	0.11	3.27	1.29	2.66	0.06	18.4	20.7	0.25	0.00	0.09	98.9	92.6
KZ15-16	Dunite	2	52.9	0.11	2.64	1.27	2.07	0.02	17.3	23.4	0.20	0.00	0.06	100	93.8
KZ15-13	Dunite	3	53.4	0.12	2.14	1.22	2.03	0.01	16.9	23.7	0.38	0.00	0.01	100	93.7
KZ14-18	Dunite	4	55.3	0.04	0.13	0.08	0.92	0.03	18.4	24.7	0.02	0.00	0.00	99.6	97.3
KZ14-09	Harzburgite-dunite	1	54.0	0.09	1.83	1.21	2.37	0.04	18.4	21.5	0.41	0.00	0.06	99.9	93.3
KZ14-24	Harzburgite	2	53.2	0.02	2.07	0.83	2.09	0.06	17.6	23.3	0.02	0.00	0.03	99.2	93.8
KZ14-01	Harzburgite	6	53.1	0.02	2.27	0.98	2.16	0.09	17.5	22.9	0.17	0.01	0.06	99.2	93.6
KZ14-08	Harzburgite	2	53.3	0.06	2.42	1.00	2.25	0.09	17.8	22.6	0.14	0.00	0.02	99.6	93.4
KZ14-10	Harzburgite	2	53.9	0.03	2.29	1.12	2.61	0.04	18.3	21.2	0.25	0.00	0.05	99.9	92.7
KZ14-11	Harzburgite	6	52.7	0.04	2.51	1.25	2.15	0.03	17.6	22.2	0.32	0.00	0.03	98.7	93.6
KZ14-13	Harzburgite	4	52.9	0.04	1.72	0.56	2.30	0.05	18.0	22.7	0.03	0.01	0.09	98.4	93.4
Purang, China															
PL14-5-20	Disseminated chromitite	3	54.2	0.00	0.77	0.49	1.53	0.09	17.5	25.0	0.07	0.00	0.08	99.7	95.4
PL14-5-18	Disseminated chromitite	5	50.9	0.11	3.47	0.97	1.78	0.05	15.7	25.0	0.33	0.02	0.05	98.4	94.1
PL14-3-1	Dunite	5	51.0	0.36	4.00	1.42	2.19	0.05	15.5	24.4	0.53	0.00	0.04	99.5	92.7
PL14-5-23	Dunite	2	50.6	0.06	2.79	0.96	1.86	0.05	16.0	24.5	0.26	0.00	0.02	97.2	93.9
PL14-5-22	Dunite	5	51.4	0.08	3.04	1.25	1.79	0.03	15.9	24.9	0.25	0.00	0.02	98.7	94.1
PL14-5-21	Dunite	4	51.5	0.07	3.47	1.36	1.94	0.06	16.0	24.4	0.30	0.00	0.06	99.2	93.7
PL14-5-14	Dunite	1	51.4	0.12	3.06	0.99	2.05	0.02	16.3	24.6	0.21	0.00	0.06	98.9	93.4
PL14-5-10	Dunite	1	53.8	0.03	1.06	0.78	1.55	0.03	17.3	24.0	0.23	0.01	0.12	99.0	95.3
PL14-5-4	Harzburgite	3	52.4	0.10	2.67	0.97	1.77	0.06	16.9	24.1	0.07	0.01	0.02	99.0	94.5

Note: * from Ahmed and Arai (2002). ** from Melcher et al. (1997). No., number of analyses.

This is a preprint, the final version is subject to change, of the American Mineralogist (MSA)
Cite as Authors (Year) Title. American Mineralogist, in press.
DOI: https://doi.org/10.2138/am-2020-7270

Table 2. Trace element compositions of clinopyroxene associated with chromite in chromitites and peridotites from Kızıldağ and Kars ophiolites.

Sample	Rock type	Ti	Sr	Y	La	Ce	Pr	Nd	Sm	Eu	Gd	Tb	Dy	Ho	Er	Tm	Yb	Lu
KZ14-01	Harzburgite	145	0.55	1.19	0.42	0.35	0.25	1.45	1.50	0.40	1.31	0.19	0.70	0.18	0.56	0.16	0.74	0.16
KZ14-23	Harzburgite	155	0.64	1.09	0.44	0.41	0.28	1.49	1.76	0.45	1.53	0.21	0.86	0.21	0.54	0.17	0.83	0.17
KZ14-25	Harzburgite	106	0.37	0.82	0.28	0.26	0.20	1.15	1.40	0.35	1.16	0.18	0.71	0.18	0.50	0.16	0.68	0.17
KZ15-09	Harzburgite-dunite	510	0.66	3.54	0.43	0.37	0.25	1.43	1.47	0.40	1.33	0.20	0.75	0.18	0.56	0.16	0.75	0.15
KZ15-10	Disseminated chromitite	1001	4.50	5.64	0.37	0.34	0.25	1.43	1.68	0.50	1.66	0.29	1.18	0.28	0.73	0.24	1.12	0.26
KZ14-27-1	Banded chromitite	1031	10.5	8.07	0.27	0.60	0.19	1.19	1.21	0.31	1.30	0.23	1.37	0.35	0.89	0.18	1.08	0.21
KZ14-32-1	Banded chromitite	449	0.87	4.79	0.39	0.36	0.26	1.49	1.70	0.45	1.47	0.22	0.89	0.22	0.75	0.19	1.10	0.20
KZ15-37	Nodular chromitite	366	11.3	12.1	0.35	0.69	0.23	1.39	1.48	0.39	1.39	0.27	1.88	0.47	1.33	0.20	1.38	0.20
KZ15-38	Massive chromitite	390	2.38	6.44	0.33	0.28	0.20	1.16	1.36	0.34	1.30	0.22	1.22	0.31	0.92	0.20	1.17	0.21
KZ15-21	Massive chromitite	437	2.50	8.03	0.43	0.39	0.27	1.47	1.68	0.43	1.39	0.20	1.30	0.32	1.01	0.17	1.26	0.19
KZ14-32-2	Massive chromitite	1064	10.7	9.37	0.29	0.46	0.21	1.21	1.30	0.37	1.31	0.23	1.69	0.39	1.14	0.18	1.13	0.19
KZ14-38	Massive chromitite	680	5.59	7.40	0.46	0.42	0.28	1.47	1.69	0.46	1.34	0.20	0.99	0.24	0.78	0.17	1.30	0.17
CIC15-13	Massive chromitite	498	4.10	3.98	0.80	0.64	0.50	2.68	2.94	0.75	2.50	0.37	1.24	0.34	0.94	0.31	1.43	0.29
CIC15-10	Massive chromitite	485	4.73	3.27	0.33	0.32	0.21	1.19	1.38	0.38	1.18	0.18	0.67	0.18	0.49	0.15	0.74	0.14

This is a preprint, the final version is subject to change, of the American Mineralogist (MSA)
Cite as Authors (Year) Title. American Mineralogist, in press.
DOI: https://doi.org/10.2138/am-2020-7270

Table 3. Li isotopic compositions of clinopyroxene in Kızıldağ chromitites.

Sample	Rock type	Mineral	δ^7Li (‰)	1se	Li (ppm)	1se
KZ14-32-2	Massive chromitite	Cpx	-1.39	1.07	0.29	0.00
		Cpx	-29.9	0.55	1.28	0.00
		Cpx	-10.5	0.69	1.87	0.02
		Cpx	-11.7	0.55	1.90	0.02
		Cpx	-10.8	0.61	2.15	0.02
		Cpx	-8.55	0.51	2.52	0.02
KZ15-38	Massive chromitite	Cpx-rim	-0.99	1.12	1.77	0.02
		Cpx-core	6.54	1.62	0.65	0.01
		Cpx-rim	0.34	1.38	0.46	0.01
		Cpx-single	-0.67	1.27	0.61	0.00
		Cpx-core	0.93	1.14	0.33	0.00
		Cpx-rim	-5.02	1.36	0.63	0.00
KZ14-38	Massive chromitite	Cpx	-1.78	1.42	0.48	0.00
		Cpx	1.62	1.60	0.49	0.02
		Cpx	-9.11	0.37	6.70	0.03

This is a preprint, the final version is subject to change, of the American Mineralogist (MSA)
Cite as Authors (Year) Title. American Mineralogist, in press.
DOI: https://doi.org/10.2138/am-2020-7270

Table 4. Water contents (ppm) of olivine (Ol), clinopyroxene (Cpx) and orthopyroxene (Opx) in rocks of the Kızıldağ ophiolite, Turkey.

Sample	Rock type	Mineral	Grain No.	H_2O
KZ14-23	Harzburgite	Ol	2	udl
		Opx	12	113
KZ15-09	Harzburgite-dunite transition	Ol	18	9
		Opx	13	59
KZ15-16	Dunite	Ol	12	24
KZ14-40	Dunite	Ol	13	42
KZ15-10	Disseminated chromitite	Ol	12	17
KZ14-32	Banded chromitite	Ol	12	19
		Cpx	3	366
		Opx	14	74
KZ15-23	Anti-nodular chromitite	Ol	10	24
KZ15-38	Massive chromitite	Ol	10	48
		Cpx	13	801
KZ15-21	Massive chromitite	Ol	12	53

Note: ndl, under detection limit.